Detruncation of Clinical CT Scans Using a Discrete Algebraic Reconstruction Technique Prior

Achim Byl[a,b], Michael Knaup[a], Magdalena Rafecas[c], Christoph Hoeschen[d], and Marc Kachelrieß[a,b]

[a]German Cancer Research Center (DKFZ), Heidelberg, Germany
[b]Heidelberg University, Heidelberg, Germany
[c]University of Lübeck, Lübeck, Germany
[d]University Magdeburg, Magdeburg, Germany

ABSTRACT

Successful image reconstruction in computed tomography (CT) relies on the completeness of the projections. If the patient does not fit in the field of measurement, the projections are truncated causing cupping artifacts in the image and a diminished field of view (FOV). In order to restore the CT values and extend the FOV, the projections have to be completed, for example via an extrapolation. The discrete algebraic reconstruction technique (DART) has shown its efficacy in reconstructing discrete images from insufficient raw data. In this work, we use DART images as a prior for projection completion of clinical CT scans. We compare our method to the conventional adaptive detruncation (ADT) and evaluate the RMSE inside and outside the FOV along with the Dice score.

Keywords: Computed Tomography, Truncation, Detruncation, Algebraic Reconstruction, DART

1. INTRODUCTION

Image reconstruction in computed tomography (CT) depends heavily on the quality of the available raw data. However, in many instances the acquisition parameters lead to raw data that are insufficient for a conventional method such as filtered back-projection (FBP). Typical problems are a low number of projections, small angular range, or low tube current. This work focuses on the issue of truncated projections, i.e. the case where the patient does not fully fit in the maximum field of view (FOV) of the scanner. In clinical practice, truncation most often occurs with obese patients, patients that are not centered properly on the table, or when using C-arm systems, which generally feature small FOVs.

Sinogram truncation is twofold problematic. On the one hand, voxels inside of the FOV suffer from cupping artifacts. On the other hand, there is a demand of artificially extending the FOV. Voxels in the extended FOV (eFOV) are of interest for several algorithms, including metal artifact reduction and beam hardening correction in CT, and attenuation and scatter correction in PET.[1,2]

In order to reduce artifacts within the FOV, several data extrapolation methods have been developed.[3–5] These conventional algorithms are able to restore the CT values within the FOV to acceptable values, such that the cupping artifacts are removed. However, voxels in the eFOV are typically not reconstructed accurately. Recently, there have also been deep learning methods developed for the purpose of extending the FOV, showing promising results.[6,7]

Another method that has shown promise for reconstructing truncated raw data is the discrete algebraic reconstruction technique (DART).[8–10] DART is a well-known algorithm for reconstructing discrete CT volumes, e.g. in the context of non-destructive testing of homogeneous objects. It was specifically developed for scans with few projections or limited angular range.[11–13] Utilizing the assumption that the object consists of very few attenuation coefficients, DART is capable of image reconstruction with severely limited data.

The corresponding author is Achim Byl. E-mail: achim.byl@dkfz.de

7th International Conference on Image Formation in X-Ray Computed Tomography,
edited by Joseph Webster Stayman, Proc. of SPIE Vol. 12304, 123041M
 · 0277-786X · doi: 10.1117/12.2646885

Table 1. RMSE and Dice values for both patients and levels of truncation. RMSE is given for the original and for the extended FOV.

		Truncated		Cosine Detruncation		ADT		DART		Our Method	
		$M_t = 678$	$M_t = 372$	$M_t = 678$	$M_t = 372$	M=678	$M_t = 372$	$M_t = 678$	$M_t = 372$	$M_t = 678$	$M_t = 372$
Patient 1	$RMSE_{FOV}$ [HU]	82.01	1005.6	28.38	92.56	15.64	38.53	124.25	141.07	**9.67**	**35.57**
	$RMSE_{eFOV}$ [HU]	145.31	788.32	72.75	275.07	42.20	152.89	108.16	163.23	**28.34**	**134.26**
	Dice	0.977	0.65	0.991	0.859	0.996	0.968	0.996	0.973	**0.999**	**0.975**
Patient 2	$RMSE_{FOV}$ [HU]	97.29	912.14	27.94	114.15	14.83	**26.79**	150.42	178.30	**12.72**	45.92
	$RMSE_{eFOV}$ [HU]	162.53	699.16	73.03	294.24	42.77	**127.81**	132.38	194.03	**34.47**	161.48
	Dice	0.9703	0.673	0.988	0.835	0.996	**0.965**	0.993	0.960	**0.999**	0.963

In this work, we apply DART to clinical CT data to obtain a prior image for detruncation, i.e. to fill the missing projections. Although clinical CT volumes are not strictly homogeneous, a typical CT scan consists only of soft tissue, bone, and air. In addition, for the purposes of the projection completion, the patient is often approximated by a single attenuation value.[3–5] Although DART was developed for discrete CT, it internally computes real valued images, which we use for detruncation. To evaluate our method, it is compared to the established adaptive detruncation (ADT).[4]

2. METHODS

We define the detruncation problem as follows. We have access to truncated parallel beam raw data $p_t(\vartheta, \xi)$ with M_t pixels of size $\Delta\xi$. Let $\xi_{t,max} = \frac{1}{2}(M_t - 1)\Delta\xi$, such that the detector range is $-\xi_{t,max} \leq \xi \leq \xi_{t,max}$. In order to reconstruct an artifact free image, the full detector should have $M_f > M_t$ pixels, corresponding to $\xi_{f,max} = \frac{1}{2}(M_f - 1)\Delta\xi$. Thus, the required extrapolation includes pixels within $\xi_{t,max} < |\xi| \leq \xi_{f,max}$. In image domain, this expands the original FOV with radius $R_{M,t} = \xi_{t,max}$ to the eFOV with radius $R_{M,f} = \xi_{f,max}$. Due to the limitations of the scanner, the eFOV cannot be larger than the bore size. Figure 1 shows our strategy to fill the missing projections: First, generate a prior image using the DART algorithm. Second, forward-project the prior image and fill in the missing data in the original sinogram using the prior sinogram.

2.1 Generating a DART Prior Image

DART employs a combination of discretization and real-valued algebraic reconstruction.[11,12] Figure 1 shows the basic DART scheme on the left. During each DART iteration, only a subset of pixels is changed, while the rest of the pixels are set to constant values. In order to determine the fixed pixels, we first segment the current image estimate into air and tissue by thresholding at -500 HU. Then, every pixel that is fully surrounded by pixels of the same class is fixed and set to a value of -1000 HU or 100 HU for air or tissue, respectively. Each pixel is given an additional probability of 65% to be classified as non-fixed, so that values inside homogeneous patches can be corrected. Subsequently, we perform five SART iterations where only the non-fixed pixels are considered.[14] One SART iteration is defined as

$$f_{new} = f + \lambda \frac{1}{X^T 1} X^T \left(\frac{p - Xf}{X1} \right), \tag{1}$$

where f is the current image estimate, f_{new} is the new estimate, p are the raw data, λ is a relaxation factor, X is the forward-projection and X^T is the back-projection.

Since the fixed pixels contain no noise, all projection noise will be distributed over the non-fixed pixels. Therefore, the last step is a smoothing with a Gaussian filter with a standard deviation of 0.5 pixels. This finishes one iteration and the algorithm continues with the segmentation step. Since there is no formal stopping criterion, we set the maximum number of iterations N_{iter} to 5000. In most cases, a few hundred iterations were sufficient. To initialize the DART algorithm, we perform a simple cosine detruncation followed by an FBP. Note that only the original raw data are used for the DART iterations.

In conventional applications, the DART result will again be segmented at the end of the algorithm, as a discrete volume is desired. In this work, DART is used with clinical data. Therefore, we omit the final thresholding and instead use the real valued image as the prior image.

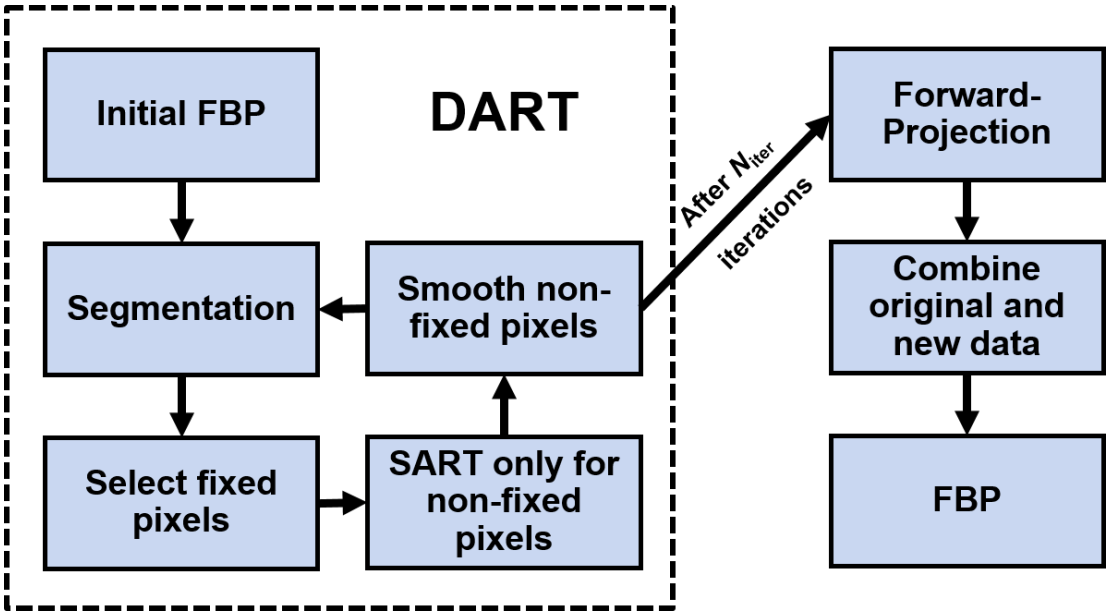

Figure 1. Scheme of the proposed DART detruncation. The dashed box highlights the DART reconstruction, the right side shows the data completion step.

2.2 Projection Completion

In order to acquire a complete sinogram, the information in the prior image and the original raw data p_t have to be combined. First, forward-project the prior image to obtain the prior sinogram p_DART. Then, the detruncated sinogram p_d incorporates the original data p_t wherever possible and p_DART otherwise. Thus, only the outer regions are filled with the prior sinogram. However, simply copying the pixel values might cause artifacts at the edge between original and new data. To amend this, a factor $c(\vartheta, \xi)$ scales the new data to match the original data at the boundary. This factor is calculated separately for each projection and side. Finally, the DART-detruncated image is reconstructed from p_d via FBP.

2.3 CT Data

All data sets were obtained with a SOMATOM Force CT scanner (Siemens Healthineers, Forchheim, Germany). Images were acquired at 70 kV, and reconstructed on a 512×512 matrix with 0.6 mm slice thickness and 0.8 mm $\times$ 0.8 mm pixel size.

We generate full and truncated sinograms by monochromatically forward-projecting in parallel beam geometry. The simulations are performed with $N = 256$ projections with an angular range of 0 to 180°. The full sinogram has $M_\mathrm{f} = 1024$ detector pixels with a pixel size of 0.5 mm. We investigate two levels of truncation with $M_\mathrm{t} = 682,\ 372$ detector pixels, which correspond to a relative detector size of $\frac{2}{3}$ and $\frac{1}{3}$, respectively. Note that our method can easily be adjusted to other geometries, e.g. fan-beam or cone-beam.

2.4 Analysis

To quantify how well the algorithm can correct CT values inside the original FOV, we calculate the root mean squared error (RMSE) within the FOV with respect to the image reconstructed from the full detector. The RMSE for an image $f(i,j)$ with respect to the ground truth image GT is defined as

$$\mathrm{RMSE} = \sqrt{\frac{1}{N_x N_y} \sum_{0 \le i,j \le N_x, N_y} (f(i,j) - \mathrm{GT}(i,j))}. \tag{2}$$

Furthermore, we compute the RMSE within the eFOV and Dice score of the whole image to compare the ability of the detruncation to restore the CT values and patient outline outside of the original FOV. For the latter, the images are segmented into air and soft tissue with a threshold of -500 HU. The Dice score is defined as

$$\text{Dice} = \frac{2\text{TP}}{2\text{TP} + \text{FP} + \text{FN}}, \tag{3}$$

where TP are the true positives, FP the false positives and FN the false negatives. To compare the DART detruncation with a conventional method, we also apply the adaptive detruncation (ADT)[4] to the data.

3. RESULTS

Figure 2 shows the first patient, including detruncation results from cosine detruncation, ADT, DART, and our method. In the left column, the scan suffers from light truncation. This causes minor cupping artifacts at the left and right side of the patient in the uncorrected FBP reconstruction. All methods have have successfully removed the cupping and restored CT values to voxels in the eFOV. After cosine detruncation, artifacts remain at the edge of the FOV and the tissue in the eFOV is too dark. In the ADT result, voxels on the right side are slightly brighter than in the other ground truth. For the case of strong truncation, displayed in the right column of Figure 2, there is a considerable difference between ADT and our method. While ADT is able to restore CT values inside the original FOV very well, the tissue outside of the FOV is too bright and the patient outline does not agree with the ground truth. In contrast, the DART-detruncated image is very close to the full-view reconstruction, although fat has been converted into water at the bottom of the image and some bone anatomy is incorrect. These findings are supported by the numerical evaluation in Table 1. In all cases, our method outperforms ADT in terms of RMSE and Dice score. Notably, the DART prior image has relatively high RMSE values (above 100 HU in all cases) but good Dice scores, indicating high image noise. Figure 4 shows the projections for the case of strong truncation. Although the ADT is able to estimate the projections approximately, the DART prior and DART detruncation are noticeably smoother and more accurate.

Figure 3 displays the results of the second patient. Again, both ADT and DART detruncation perform well when the data are only mildly truncated. As for the first case, the ADT image features slightly too high CT values on the right side. The DART prior image and DART-detruncated image show a dark streak along the edge of the FOV. For strong truncation, the ADT again yields CT values that are too high on the left and right side of the FOV and does not provide a clear patient outline. Still, ADT clearly outperforms the cosine detruncation. While the DART reconstruction gives more accurate CT values in general, there are gaps in the soft tissue of the patient. This artifact is also evident in the RMSE of the eFOV and the Dice score, which are lower than ADT for both the DART and DART-detruncated image. In the case of mild truncation, our method still yields superior numerical results.

4. DISCUSSION & CONCLUSION

In this work, we propose a method of CT raw data detruncation based on the DART reconstruction. The DART detruncation was capable of reducing cupping artifacts in the FOV, as well as restoring CT values in the eFOV, for two levels of truncation. Compared to the conventional ADT, our method produced superior visual and numerical results. However, for patient 2 with strong truncation, some anatomy was incorrectly reconstructed as air, yielding worse numerical results than ADT. These artifacts would likely be prevented with a better initial estimate of the image, along with additional iterations of DART.

This work uses the original DART algorithm[11,12] with a single, manually determined threshold. In the future, a more refined version of DART, e.g. with automatic parameter optimization or improved performance for noisy projections[13,15,16] should be preferred, in order to reduce computation time and image noise.

Acknowledgment

This work is supported by the German Federal Ministry for the Environment, Nature Conservation, Nuclear Safety and Consumer Protection (BMUV) under grant 67KI2036B. Parts of the reconstruction software were provided by RayConStruct®GmbH, Nürnberg, Germany.

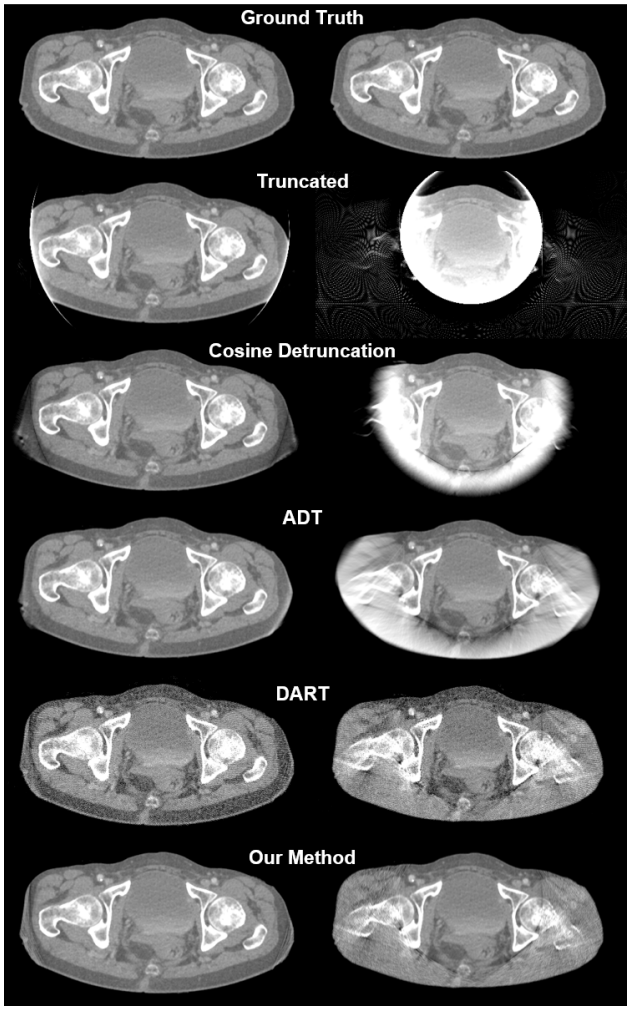

Figure 2. Detruncation results for Patient 1. Left column shows mild truncation ($M_{\mathrm{t}} = 682$), right column strong truncation ($M_{\mathrm{t}} = 372$). Top to bottom: ground truth, truncated FBP, cosine detruncation, ADT, DART prior image, DART detruncation. $C = 0$ HU, $W = 1000$ HU.

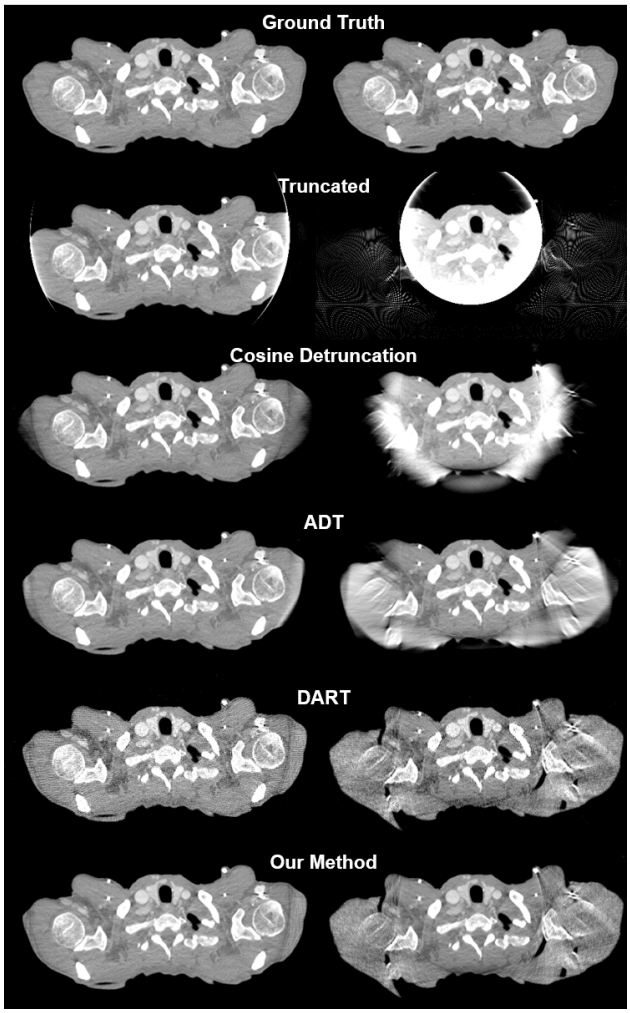

Figure 3. Detruncation results for Patient 2. Left column shows mild truncation ($M_{\mathrm{t}} = 682$), right column strong truncation ($M_{\mathrm{t}} = 372$). Top to bottom: ground truth, truncated FBP, cosine detruncation, ADT, DART prior image, DART detruncation. $C = 0$ HU, $W = 1000$ HU.

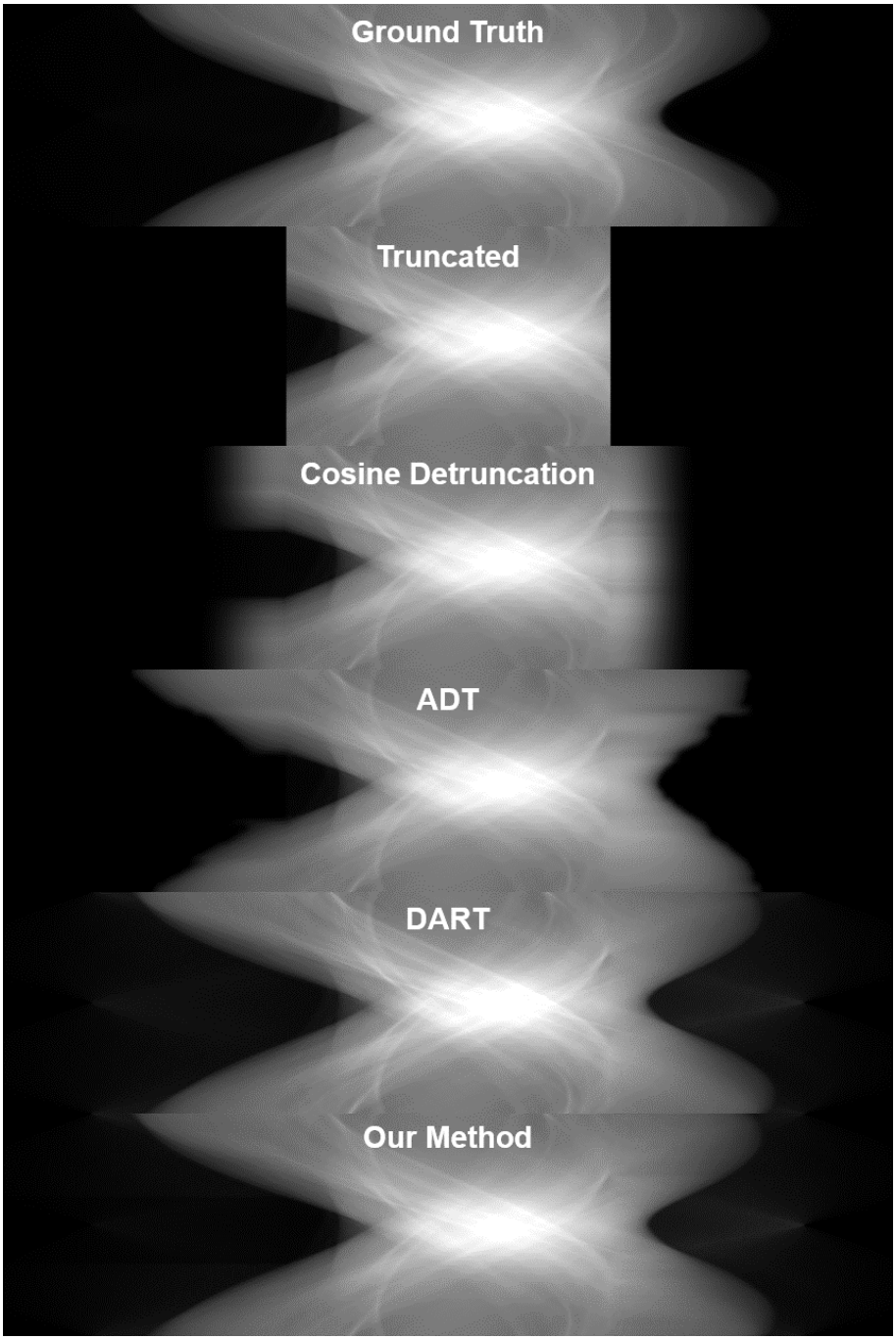

Figure 4. Projections for Patient 1 with strong truncation after detruncation. Top to bottom: ground truth, truncated FBP, cosine detruncation, ADT, DART prior image, DART detruncation.

REFERENCES

[1] Shi, L., Bennett, N. R., Shiroma, A., Sun, M., Zhang, J., Colbeth, R., Star-Lack, J., Lu, M., and Wang, A. S., "Single-pass metal artifact reduction using a dual-layer flat panel detector," *Medical Physics* **48**(10), 6482–6496 (2021).

[2] Žabić, S., He, L., and Bao, Y., "A method for reduction of axial truncation artifacts," in [*CT Meeting 2020 Proceedings*], 158–161 (2020).

[3] Hsieh, J., Chao, E., Thibault, J., Grekowicz, B., Horst, A., McOlash, S., and Myers, T., "A novel reconstruction algorithm to extend the CT scan field-of-view," *Medical Physics* **31**(9), 2385–2391 (2004).

[4] Sourbelle, K., Kachelrieß, M., and Kalender, W. A., "Reconstruction from truncated projections in CT using adaptive detruncation," *European Radiology* **15**(5), 1008–1014 (2005).

[5] Maltz, J. S., Bose, S., Shukla, H. P., and Bani-Hashemi, A. R., "CT truncation artifact removal using water-equivalent thicknesses derived from truncated projection data," in [*2007 29th Annual International Conference of the IEEE Engineering in Medicine and Biology Society*], 2907–2911, IEEE (2007).

[6] Fonseca, G. P., Baer-Beck, M., Fournie, E., Hofmann, C., Rinaldi, I., Ollers, M. C., van Elmpt, W. J., and Verhaegen, F., "Evaluation of novel AI-based extended field-of-view CT reconstructions," *Medical Physics* (2021).

[7] Huang, Y., Gao, L., Preuhs, A., and Maier, A., "Field of view extension in computed tomography using deep learning prior," in [*Bildverarbeitung für die Medizin 2020*], 186–191, Springer (2020).

[8] Van Gompel, G., Defrise, M., and Batenburg, K. J., "Reconstruction of a uniform star object from interior x-ray data: Uniqueness, stability and algorithm," *Inverse Problems* **25**(6), 065010 (2009).

[9] Van Gompel, G., [*Towards Accurate Image Reconstruction from Truncated X-Ray CT Projections*], Universiteit Antwerpen, Faculteit Wetenschappen, Departement Fysica (2009).

[10] Banjak, H., Costin, M., Vienne, C., Guillamet, R., and Kaftandjian, V., "Iterative CT reconstruction on limited angle trajectories applied to robotic inspection," in [*AIP Conference Proceedings*], **1806**(1), 020009, AIP Publishing LLC (2017).

[11] Batenburg, K. J. and Sijbers, J., "DART: a fast heuristic algebraic reconstruction algorithm for discrete tomography," in [*2007 IEEE International Conference on Image Processing*], **4**, IV133–IV136, IEEE (2007).

[12] Batenburg, K. J. and Sijbers, J., "DART: a practical reconstruction algorithm for discrete tomography," *IEEE Transactions on Image Processing* **20**(9), 2542–2553 (2011).

[13] Yang, F., Zhang, D., Huang, K., Gao, Z., and Yang, Y., "Incomplete projection reconstruction of computed tomography based on the modified discrete algebraic reconstruction technique," *Measurement Science and Technology* **29**(2), 025405 (2018).

[14] Andersen, A. H. and Kak, A. C., "Simultaneous algebraic reconstruction technique (SART): a superior implementation of the ART algorithm," *Ultrasonic Imaging* **6**(1), 81–94 (1984).

[15] van Aarle, W., Batenburg, K. J., and Sijbers, J., "Automatic parameter estimation for the discrete algebraic reconstruction technique (DART)," *IEEE Transactions on Image Processing* **21**(11), 4608–4621 (2012).

[16] Zhuge, X., Palenstijn, W. J., and Batenburg, K. J., "TVR-DART: A more robust algorithm for discrete tomography from limited projection data with automated gray value estimation," *IEEE Transactions on Image Processing* **25**(1), 455–468 (2016).